Dear author,

In the stage of preparing your full work for evaluation, after receiving approval of the corresponding abstract, we kindly ask you to follow the next steps:

1. Update your approved abstract (you might want to introduce modifications) and submit it now in a written version according to the abstract template (many abstracts were introduced directly into the websystem). This version of the abstract will compose the *abstracts booklet* to be distributed to the participants when registering;

2. Fill the form in the next page, indicating to which section you would like your work to be directed. This will help organizing the sessions according to the mini-symposia advertised rather than in the areas and subareas present in the websystem. We apologize for this possible confusion. The reason is that we are using the websystem provided by ABCM, which does not allow us to introduce thematic sessions freely.

If any doubts arise, please contact us.

Your presence in MecSol 2017 will help making this a very successful event. We look forward to seeing you in Joinville!

With kind regards,

The Organizing Committee
MecSol 2017

6th International Symposium on Solid Mechanics

Click on the box to select the Mini-Symposia:

☒ Multiaxial and Fretting Fatigue (*Edgar Mamiya* and *Lucival Malcher*);

☐ Composite Materials (*Ricardo de Medeiros*);

☐ Constitutive Models I – Plasticity and Damage (*Lucival Malcher*, *Miguel Vaz Jr.* and *Edgar Mamiya*);

☐ Constitutive Models II – Viscoelastic and Viscoplastic Solids: Models and Applications (*Heraldo Mattos*);

☐ Impact Engineering (*Marcílio Alves*);

☐ Structural Reliability Methods and Reliability-Based Design Optimization (*André Beck*);

☐ Topology Optimization of Multifunctional Materials, Fluids and Structures (*Eduardo Lenz Cardoso* e *Emilio Carlos Nelli Silva*);

☐ Topological Derivatives: Theory and Applications (*André Novotny*);

☐ X-FEM, G-FEM and Meshfree Methods (*Roberto Dalledone Machado* and *Rodrigo Rossi*);

☐ High Order Finite Elements (*Marco Lúcio Bittencourt*);

☐ Nonlinear Analyses (*Eduardo Campello*);

☐ Other section;

Investigations on fretting fatigue crack nucleation in a cylinder on flat contact via multiaxial fatigue models

Fernando Salles da Silva Pires
Mechanic Engineering Department
Pontifical Catholic University of Rio de Janeiro
fernandopires@aluno.puc-rio.br

Jaime Tupiassú Pinho de Castro
Mechanic Engineering Department
Pontifical Catholic University of Rio de Janeiro
jtcastro@puc-rio.br

Luiz Carlos Rolim Lopes
Mechanic Engineering Department
EEIMVR – Federal Fluminense University
luiz.crolim@uol.com.br

ABSTRACT

This paper focuses on the prediction of crack nucleation under fretting fatigue loadings via multiaxial fatigue models for a couple of steel. In this work, numerical model of a two-dimensional cylinder on flat contact, which allows applying fretting and fatigue efforts was built using Abaqus application. Kujawaski's critical-plane tensile-based model (SWT_D) and Findley's critical-plane shear-based model (F) were used to predict crack nucleation risk and were compared to the commonly models used in the literature for the same purpose such as Smith-Watson-Topper (SWT) critical-plane tensile based model and Crossland's invariant-based model. Besides the crack nucleation risk analysis, finite life was estimated using Basquin`s law for each model. The numerical results have been compared among them and to the experimental results available in the literature.

In case of elastic contact, the results predicted by SWT_D and Findley's models show good agreement with the experimental results. Nevertheless, the SWT_D model does not reproduce the physics of fretting fatigue cracking which was better achieved by Findley's model.

For the experimental data set with the higher contact pressure, where plastic strain dominates (LCF), SWTD parameter shows good agreement with the experimental results when calculated at the contact bord. Furthermore, both SWT_D and SWT parameters yields similar results as the local mean stress are moderately negative. The advantage on the use of these critical-plane parameters is that they do not require the definition of a critical length. Such issue is the great challenge of non-local strategies. However, finding the critical-plane is a task requiring an exhaustive search among all combinations of candidate planes.

Non-local strategies combined with multiaxial models such as Crossland's model have been considered by many authors to predict crack nucleation under fretting fatigue loadings. The calculation of Crossland's damage parameter as an invariant stress-based model is straightforward and does not require the critical-plane search. On the other hand, identifying the critical length to calibrate this model can be a problem in case of lack of experimental results. For the couple of steel investigated in this work, the use of Crossland's model combined with a critical length calculated via point method proposed by Taylor has produced non-conservative predictions. Nevertheless, considering half-critical length ($L_{PM}/2$), the predictions correlated well with the experimental results.

Keywords: Fretting fatigue, multiaxial fatigue, finite elements, crack nucleation, steel.

1 INTRODUCTION

Fretting is a physical phenomenon that appears when a contact between two parts is subjected to micro-displacements. These displacements can induce wear (gross slip) and/or cracking (partial slip) of the interfaces. Combined with cyclic fatigue loading, fretting fatigue can induce crack propagation that can reduce the endurance of the assembly [1].

Fretting fatigue may occurs in many engineering assemblies as riveted joints, dove-tail section of jet engines, interwire contact in cables [2] and most recently it has been investigated in pressure armour layer of dynamic flexible pipes [3].

Fretting fatigue usually displays high stress gradient that affect observed lives. In fretting fatigue, the component will often experience a very severe stress state at the surface, but this decays rapidly away from the surface over length scales comparable with many material microstructures [4].

Fretting fatigue crack nucleation is usually predicted from multiaxial models combined with non-local strategies to take into account the stress gradient. Farris et al introduced the multiaxial fatigue model proposed by Smith-Watson-Topper to calculate the risk of crack nucleation under fretting fatigue loadings [5].

Following the idea of effective stress introduced by Taylor [6] in occurrence of stress gradient, non-local approaches have received considerable attention in the literature. Araújo et al has demonstrated that good prediction can be obtained if the effective stress is calculated at a critical distance, which is defined as half crack length at the transition between short and long cracks [7].

Crossland-invariant based model combined with a critical distance strategy has been used by many authors to predict crack nucleation under fretting fatigue loadings [8-10]. Nevertheless, the definition of such a distance can be difficult in case of lack of experimental results.

From an engineering standpoint, it is important to have a model to predict the risk of crack nucleation in a simple and reliable way. This paper intends to explore the prediction of fretting fatigue crack nucleation via multiaxial fatigue models. A bi-dimensional finite element model was created with commercial software Abaqus. The resulting elastoplastic stress/strain field is combined with multiaxial models critical-plane based to perform such a prediction. Critical-plane approach can describe much better than invariant-based models the fatigue behavior of directional-damage materials, which fail due to a single dominant crack.

2 STRESS ANALYSIS IN THE CONTACT

The real contacts where fretting fatigue occurs are complex. Nevertheless, when testing at laboratory, the contact is in general simplified being the cylinder on flat contact (focus of this work), one of the configuration most used for fretting fatigue tests. The cylinder on flat contact is illustrated schematically in Figure 1.

In studying the fretting problem, most researches assume contact on the Hertz or non-conformal contact model [11]. Non-conforming contact refers to the condition that the size of the contact zone is generally much smaller than the characteristics dimension of the contacting bodies.

In case of partial slip regime, where cracking is the predominant failure mode, the tangential load Q for each time verifies the $Q < \mu P$ (μ is the friction coefficient and P the normal load).

The partial slip problem in elastic condition was solved by Mindlin and Cattaneo and gives the pressure distribution p(x) and the shear stress distribution q(x) at the contact surface. The distribution of stress at the contact surface is illustrated in Figure 1.

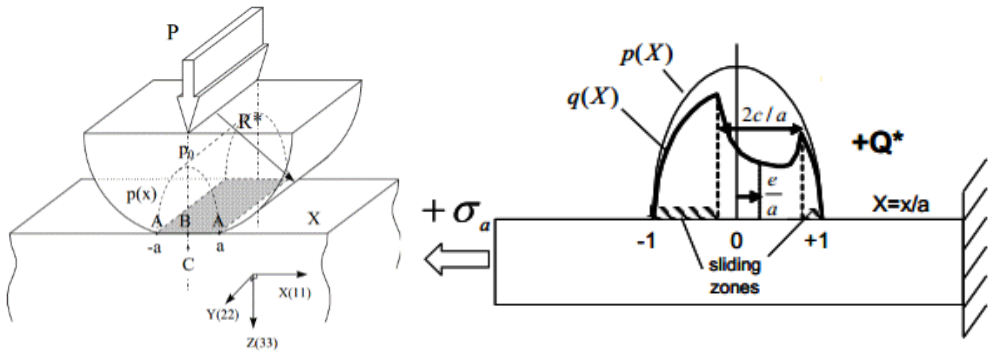

Figure 1 – Cylinder on flat configuration and schematic view of pressure distribution p(x) and shear stresses distribution q(x) at the contact surface.

2.1 Pressure field at the surface

For similar materials, the pressure distribution at the surface is not affected by the shear stresses (in elastic contact) and can be written as:

$$p(x) = p_0\sqrt{1-(x/a)^2} \tag{1}$$

where p_0 is the maximal Hertzian pressure and a is the semi contact width.

2.2 Shear stress at the surface

In case of fretting fatigue loadings, the shear stress distribution at the surface is given by:

$$f(x) = \begin{cases} q_0\sqrt{1-(x/a)^2}, & if\ -a \le -c+e \\ q_0\left[\sqrt{1-(x/a)^2} - c/a\sqrt{1-(x-e/c)^2}\right], & if\ -c+e \le x \le c+e \\ q_0\sqrt{1-(x/a)^2}, & if\ c-e \le x \le a \end{cases} \tag{2}$$

where q_0 is the maximal interfacial shear stress, c being the semi sticking zone width and e is the offset of the stick zone from the center of the contact introduced by fatigue loading. The eccentricity in the stick zone can be written as:

$$e = \left[\frac{a}{8q_0}\sigma_{max}(1-R)\right] \tag{3}$$

Equation (2) provides the shear surface traction when Q= Q_0 but the surface shear traction can be computed at any instant of the tangential load cycle as demonstrated in reference [12]. Once the surface tractions are known, the elastic subsurface stress field can be computed using the equations available in [11].

2.3 Multiaxial fatigue models and fretting fatigue

Mechanic contact under fretting fatigue loadings is typically a multiaxial problem. At the trailing contact bord (x=-a, z=0) the stress state is biaxial and proportional. Otherwise, the stress state is highly multiaxial and non-proportional.

Assuming plane strain state, the complex three-dimensional problem is reduced into an equivalent two-dimensional problem. In the 9D representation, only four components are required to describe the state of stress at the contact as per equation (4).

$$\vec{\sigma} = \begin{bmatrix} \sigma_{xx} & 0 & \tau_{xz} \\ 0 & \sigma_{yy} & 0 \\ \tau_{xz} & 0 & \sigma_{zz} \end{bmatrix} \text{ being } \sigma_{yy} = \upsilon \cdot (\sigma_{xx} + \sigma_{zz}) \tag{4}$$

2.4 Critical plane models

The multiaxial models considered in this work to predict the fretting crack nucleation, Findley (F), Smith-Watson-Topper (SWT) and Kujawski (SWT_D) are based on the critical-plane approaches. These models assume for directional-damage materials that fatigue lives can be calculated from the damage at the critical-plane of the critical point where the damage induced by the loading is maximized, and that the damage on all other planes does not matter. Such critical-plane models assume that crack is driven by the ranges $\Delta\tau''_{xz}$, $\Delta\tau''_{yz}$, $\Delta\gamma''_{xz}$, $\Delta\gamma''_{yz}$ helped by the range, mean or maximum value of the normal stress σ''_z and normal strain ϵ''_z. The stresses components at the critical plane are illustrated in Figure 2.

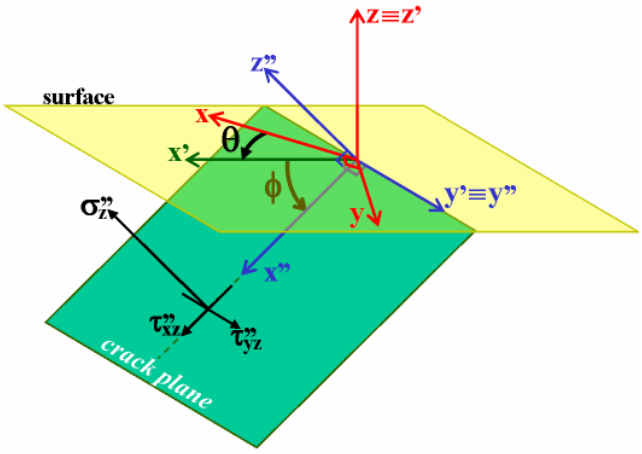

Figure 2 – Stresses acting on the critical-plane assuming that z is perpendicular to the contact surface [13].

The main calculation challenge is to compute the accumulate damage in many candidate planes at the critical point, to find the direction of the critical one where it is maximized (and thus the crack is expected to initiate).

The stress at the critical plan can be determined through the Voigt-Mandel's vector, which is equivalent to the tensorial representation. The stresses and strains projected onto a candidate plane (θ, ϕ) becomes:

$$\begin{aligned}
\tau_{yz}^{"} &= -\frac{1}{2}[\sigma_{11} sen(2\theta)\sin(\varphi) - \sigma_{22} sen(2\theta)\sin(\varphi) + 2\sigma_{13} cos(\varphi)\sin(\theta)] \\
\tau_{xz}^{"} &= \frac{1}{2}[\sigma_{11} sen(2\varphi) cos^2(\theta) + \sigma_{22} sen(2\varphi)\, sen^2(\theta) - \sigma_{33} sin(2\varphi) + 2\sigma_{13} cos(2\varphi)\cos(\theta)] \\
\sigma_z^{"} &= \sigma_{11} cos^2(\theta)\, sen^2(\varphi) + \sigma_{22} sen^2(\theta)\, sen^2(\varphi) + \sigma_{33} cos^2(\varphi) + \sigma_{13} sen(2\varphi)\cos(\theta)
\end{aligned} \tag{5}$$

$$\begin{aligned}
\gamma_{yz}^{"} &= -\frac{1}{2}[\varepsilon_{11} sen(2\theta)\sin(\varphi) + 2\varepsilon_{13} cos(\varphi)\sin(\theta)] \\
\gamma_{xz}^{"} &= \frac{1}{2}[\sigma_{11} sen(2\varphi) cos^2(\theta) - \varepsilon_{33} sin(2\varphi) + 2\varepsilon_{13} cos(2\varphi)\cos(\theta)] \\
\varepsilon_z^{"} &= \varepsilon_{11} cos^2(\theta)\, sen^2(\varphi) + \varepsilon_{33} cos^2(\varphi) + \varepsilon_{13} sen(2\varphi)\cos(\theta)
\end{aligned} \tag{6}$$

To find the maximum accumulated damage, a 10° discretization on the candidate planes, frequently used in practice, was considered ($0°<\phi<90°$, $0°<\theta<360°$). For each (θ, ϕ) candidate plane, the accumulated tensile damage and the accumulated shear damage are calculated. The maximum damage value defines the failure mode (tensile or shear), the fatigue crack nucleation life and the expected initiation direction, which should be along the plane that maximized accumulate damage.

At the trailing contact bord (x=-a, z=0) the stress state is biaxial and proportional being the shear components $\tau_{xz} = \tau_{xz} = 0$. Hence, the search space of the candidate plane can be narrowed down. The critical plane search on a free surface only needs to consider (θ, ϕ) candidate planes in the reduced domain ($0°<\phi<90°$, $0°<\theta<180°$). Banantine and Socie [14] narrowed down even further the search space of the critical plane. In case of shear components $\tau_{xz} = \tau_{xz} = 0$ and $\Upsilon_{xz} = \Upsilon_{xz} = 0$, the stress and strain projected on the candidate plane (θ, ϕ) becomes:

$$\begin{aligned}
\tau_A &= -\frac{1}{2}[\sigma_{11} sen(2\theta)\sin(\varphi) - \sigma_{22} sen(2\theta)\sin(\varphi) + 2\sigma_{13} cos(\varphi)\sin(\theta)] \\
\tau_B &= \frac{1}{2}[\sigma_{11} sen(2\varphi) cos^2(\theta) + \sigma_{22} sen(2\varphi)\, sen^2(\theta) - \sigma_{33} sin(2\varphi) + 2\sigma_{13} cos(2\varphi)\cos(\theta)] \\
\sigma_\perp &= \sigma_{11} cos^2(\theta)\, sen^2(\varphi) + \sigma_{22} sen^2(\theta)\, sen^2(\varphi) + \sigma_{33} cos^2(\varphi) + \sigma_{13} sen(2\varphi)\cos(\theta)
\end{aligned} \tag{7}$$

$$\begin{aligned}
\gamma_A &= -\frac{1}{2}[\varepsilon_{11} sen(2\theta)\sin(\varphi) + 2\varepsilon_{13} cos(\varphi)\sin(\theta)] \\
\gamma_B &= \frac{1}{2}[\sigma_{11} sen(2\varphi) cos^2(\theta) - \varepsilon_{33} sin(2\varphi) + 2\varepsilon_{13} cos(2\varphi)\cos(\theta)] \\
\varepsilon_\perp &= \varepsilon_{11} cos^2(\theta)\, sen^2(\varphi) + \varepsilon_{33} cos^2(\varphi) + \varepsilon_{13} sen(2\varphi)\cos(\theta)
\end{aligned} \tag{8}$$

The stress/strain under the free-surface condition are illustrate in Figure 3.

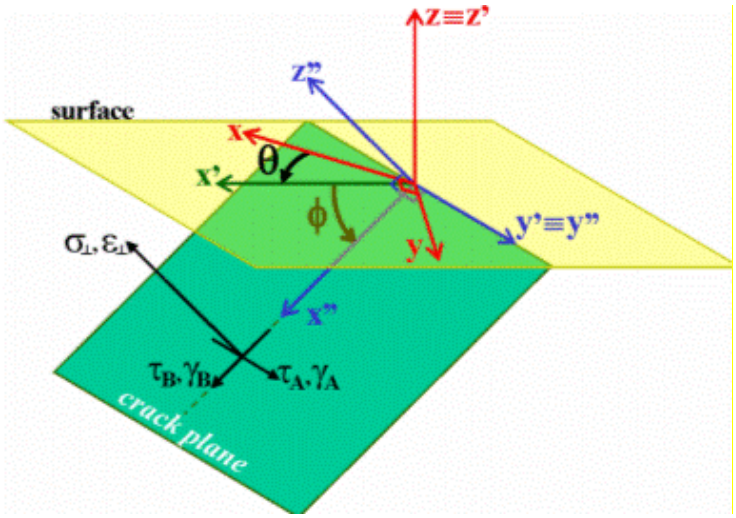

Figure 3 - Coordinates transformation assuming that z is perpendicular to the contact surface [13].

2.4.1 Findley's model

Findley`s damage parameter [15], used for multiaxial fatigue under any type of loading, is given by the maximization problem described in equation (9).

$$d_F = max_{\theta,\varphi}[\Delta\tau_F(\theta,\varphi)/2 + \alpha_F\sigma_{\perp max}(\theta,\varphi)] \tag{9}$$

where the Findley`s stress scale factor (SSF) $\alpha_F$ and Findley`s fatigue limit β_F must be calibrated from measurements in at least two types of fatigue tests (e.g. bending and cyclic torsion).In this work, this parameters were calculated as per equation (10).

$$\alpha_F = \frac{1-\frac{1}{2}\frac{S_L}{\tau_L}}{\sqrt{\frac{S_L}{\tau_L}-1}} \qquad \beta_F = S_L\frac{\frac{1}{2}}{\sqrt{\frac{S_L}{\tau_L}-1}} \tag{10}$$

where S_L is the fully reversed uniaxial fatigue limit and τ_L is the shear fatigue limit. Combined with Basquin`s law, finite life can be estimated using Findley' model as per equation (9).

$$N_F = \frac{1}{2}\left[\frac{\Delta\tau_F(\theta,\varphi)/2 + \alpha_C\sigma_{hmax}(\theta,\varphi)}{(\beta_F/\tau_L)\sigma_f}\right]^{1/b} \tag{11}$$

Findley's model is shear based, since its main cyclic damage parameter is the shear range $\Delta\tau_F$ and not $\Delta\sigma_\perp$.

2.4.2 Smith-Watson-Topper's model (SWT)

Smith-Watson-Topper`s advocated that the product of $\sigma_{\perp max}\Delta\varepsilon_{\perp}$ controls the fatigue life. The multiaxial version SWT model [16] can be written as the following maximization problem:

$$d_{SWT} = max_{\theta,\varphi}\left[\sigma_{\perp max}(\theta,\varphi)\cdot\frac{\Delta\varepsilon_{\perp}(\theta,\varphi)}{2}\right] \tag{12}$$

The non-cracking condition is given by:

$$d_{SWT} \leq d_{CI} = \frac{S_L^2}{E} \tag{13}$$

where d_{CI} is the critical value related to crack initiation condition at 10^6 cycles. The finite life version for SWT model can be written as:

$$d_{SWT} = \frac{\sigma_f^2}{E}(2N)^{2b} + \sigma_f\varepsilon_f(2N)^{2b+c} \tag{14}$$

2.4.3 Kujawaski's model (SWT_D)

To deal with large compressive mean stresses, Kujawski [17] proposed a deviatoric version of the SWT damage parameter, replacing the normal stresses and strains with their deviatoric components. When applied to the critical-plane approach, the SWT_D damage equation becomes:

$$d_{SWTD} = max_{\theta,\varphi}\left[s_{\perp max}(\theta,\varphi)\cdot\frac{\Delta e_{\perp}(\theta,\varphi)}{2}\cdot\frac{9}{4(1+\bar{\nu})}\right] \tag{15}$$

where $\bar{\nu}$ = 0.4 is the effective Poisson ratio. The deviatoric components are obtained after subtracting the maximum hydrostatic stress σ_{hmax} and $\Delta\varepsilon_h$ at the critical point.

$$s_{\perp}(\theta) = \sigma_{\perp}(\theta) - \sigma_{hmax} \text{ and } \Delta e_{\perp}(\theta) = \epsilon_{\perp}(\theta) - \Delta\epsilon_h \tag{16}$$

$$\sigma_h = (\sigma_{11} + \sigma_{22} + \sigma_{33})/3 \text{ and } \epsilon_h = (\epsilon_{11} + \epsilon_{22} + \varepsilon_{33})/3 \tag{17}$$

The non-cracking condition is given by:

$$d_{SWTD} \leq d_{CI} = \frac{S_L^2}{E} \tag{18}$$

The finite life version for SWT_D model can be written as:

$$d_{SWTD} = \frac{\sigma_f^2}{E}(2N)^{2b} + \sigma_f\varepsilon_f(2N)^{2b+c} \tag{19}$$

Figure 4 illustrates schematically the damage parameters used in the previously presented multiaxial fatigue models.

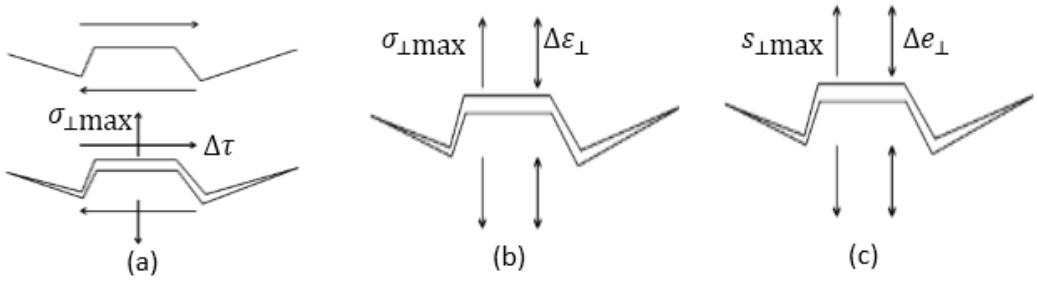

Figure 4 – Damage parameters that affect the multiaxial models investigated in this paper. (a) Findley (b) SWT and (c) SWT_D.

2.5 Invariant based model

2.5.1 Crossland's model

Crossland' model [18] is an invariant-based failure model which assumes that damage is caused by the linear combination of Mises shear stress ($\Delta\tau_C$) with the maximum component of the hydrostatic stress (σ_{hmax}). The non-cracking condition is expressed by:

$$\Delta\tau_C/2 \ + \alpha_C \, \sigma_{hmax} \ < \beta_C \tag{20}$$

where and the adjustable material constants α_C and β_C are respectively Crossland's coefficient and shear fatigue limit, which can be written as:

$$\alpha_C = \frac{\tau_L - \frac{S_L}{\sqrt{3}}}{\frac{S_L}{3}} \qquad \beta_C = \tau_L \tag{21}$$

The left side of equation (20) represents Crossland stresses, which can be written as:

$$\sigma_C = \Delta\tau_C/2 \ + \alpha_C \, \sigma_{hmax} \tag{22}$$

To estimate the risk of crack nucleation, the following scalar parameter is defined:

$$d_C = \frac{\Delta\tau_C/2}{\beta_C - \alpha_C \, \sigma_{hmax}} \tag{23}$$

The cracking condition is then expressed as:

- If $d_C \geq 1$, there is a risk of crack nucleation;
- If d_C remains less than 1, there is no risk of crack nucleation.

A finite life version of Crossland's model based on Basquin's shear-based equation is given by:

$$N_C = \frac{1}{2}\left[\frac{\Delta\tau_C/2 \ + \alpha_C \sigma_{hmax}}{(\beta_C/\tau_L)\sigma_f}\right]^{1/b} \tag{24}$$

2.6 Critical distance

To account for the gradient stress, the non-local approaches are commonly used on the prediction of fretting fatigue crack nucleation. The critical distance approach has been used by many researches [7, 9-10]. First introduced by Taylor [6], the central idea of critical distance theory approach (TCD) is the definition of an effective stress based on an average procedure over a volume surrounding the stress raiser, which is representative of the linear elastic stress field into the fatigue process zone.

Through this approach, fretting fatigue failure is expected to occur if the effective stress exceeds a reference material strength. In this work, the point method (PM) strategy was considered. According to the L_{PM}, the effective stress must be calculated at a point at a distance L_{PM} beneath the hotspot, where L_{PM} is given by:

$$L_{PM} = \frac{1}{2\pi}\left(\frac{\Delta K_0}{S_L}\right)^2 \tag{25}$$

3 MATERIALS AND EXPERIMENTAL DATA

The couple of steel investigated in this work was a low carbon steel alloy AISI 1034 (plan) and a chromium 52100 steel (cylindrical pad). Mechanical and fatigue properties for this couple of steel is presented in Table 1.

Table 1 - Mechanical and fatigue properties of the materials

Componente	Material	E (GPa)	ν	S_Y(MPa)	S_U(MPa)	S_L(MPa)	τ_L(MPa)	ΔK_0 (MPa m$^{-1/2}$)
Plane	AISI 1034	200	0.3	350	600	270	170	7
Cylinder	52100	210	0.3	1700	2000	-	-	

E: Young's modulus; ν: Poisson's coefficient; S_Y: Yield strength; S_R: Ultimate Strength; S_L: tensile fatigue limit (R = - 1); τ_L torsional fatigue limit (R = -1); ΔK_0 : long crack threshold (R = - 1).

Fatigue properties were needed to solve the finite life version of each multiaxial model. Since no specific properties were reported by the researches in reference [8], the following estimations were considered for the elastic constants:

$$\sigma_f = 1.5S_U \text{ and } b = -\log(\sigma_f/\tau_L)\,/\,\log(2N_L) \text{ where } N_L = 10^6 \text{ cycles.} \tag{26}$$

The plastic constants were taken from a similar low carbon steel alloy presented in reference [19]. The Coffin-Manson's elastic and plastic coefficients and exponents are summarized in Table 2.

Table 2 – Estimates of Coffin-Manson's elastic and plastic coefficients and exponents.

σ_f	b	ε_f	c
900	-0,115	-0,0	-0,606

Figure 5 presents the AISI 1034 stress/strain curve for monotonic uniaxial tensile loading, which can be found in reference [20].

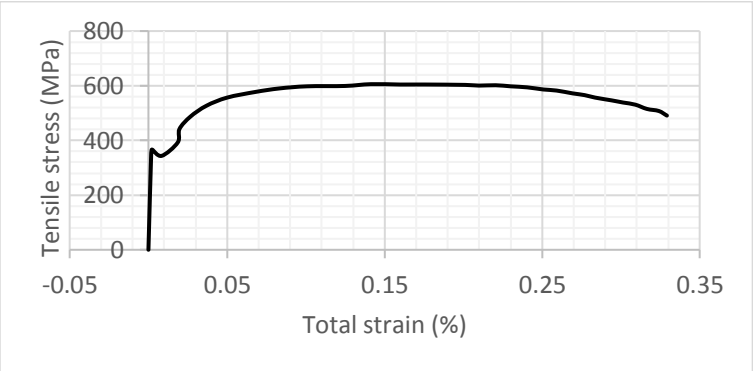

Figure 5 – Nominal monotonic stress x strain curve (AISI 1034).

For the materials investigated, plain fretting and fretting fatigue small-scale tests presented in Table 3 available in the literature [8, 10] were used to calibrate the critical distance via Crossland model as demonstrated in section 5.

Table 3 - Small-scale test results - cylinder (AISI 1034) on flat contact (52100).

ID	R*(mm)	P_L (N/mm)	Q*(N/mm)	σ_a (MPa)	p_0 (MPa)	L_p (μm)
F01	40	227	90	0	450	0
F02	40	227	98	0	450	0
F03	40	227	126	0	450	24
F04	40	227	137	0	450	29
F05	40	227	144	0	450	31
F06	40	227	146	0	450	52
F07	40	227	151	0	450	55
F08	40	227	164	0	450	65
F09	40	227	169	0	450	68
F10	40	540	206	0	700	0
F11	40	540	242	0	700	14
F12	40	540	278	0	700	77
F13	40	540	280	0	700	61
F14	40	540	283	0	700	75
FF01	40	227	145	120	450	344
FF02	40	227	125	120	450	290
FF03	40	227	100	120	450	59
FF04	40	227	125	130	450	Failure
FF05	40	227	100	130	450	Failure

R*: Cylinder radius; P_L: linear normal force; Q*: amplitude of the linear tangential force; σ_a: fatigue stress amplitude (R = -1), p_0: maximum value of Hertzian pressure distribution, a_H: Hertzian contact width, L_P: crack projected length.

Note that this set of experimental dada includes two Hertzian contact pressure being the lower pressure LP = 450 MPa and the higher pressure HP=700 MPa. The elastic assumption can be verified through the ratio p_{max}/S_y. If p_{max}/S_y < ~1.6 the contact can be considered elastic, otherwise plastic deformations are expected [11]. Therefore, for LP the contact is elastic and for the HP plastic deformation is expected. Thus, the plastic deformation was investigated in case of HP.

About the morphology of the cracks presented in Table 3, the cracks are systematically observed at the contact bord and orientated toward the inner part of the contact with an angle of about (30 ± 3) ° to the normal surface.

The analysis of the material properties indicates that the AISI 1034 is tensile-sensitive ($S_L = 270\,MPa < \tau_L\sqrt{3} = 294\,MPa$). This means that tensile cracks are most likely in such tensile-sensitive materials. Hence, for tensile sensitive materials, it is more appropriated to use models that explicitly includes $\Delta\sigma_\perp$ such as SWT, SWT_D. As the fretting crack initiates by shear stresses, Findley`s model, which is shear-based was also considered in this work. This justifies the critical-plane based models used in this work.

4 METHODOLOGY

A bi-dimensional plane strain cylinder on flat contact was developed using commercial Abaqus software, which allows the application of fretting (normal and tangential) and fatigue loadings. The mesh is composed of triangular (CPE3) and quadratic (CPE4R) linear elements.

The contact is described by a master slave algorithm and the tangential loading is determined by Lagrange multipliers through a constant friction coefficient FCO = 0.9 (sliding transition).

At the contact zone, a square partition of about 1400 µm was defined from which the stress path are extracted and the multiaxial fatigue analysis is performed.

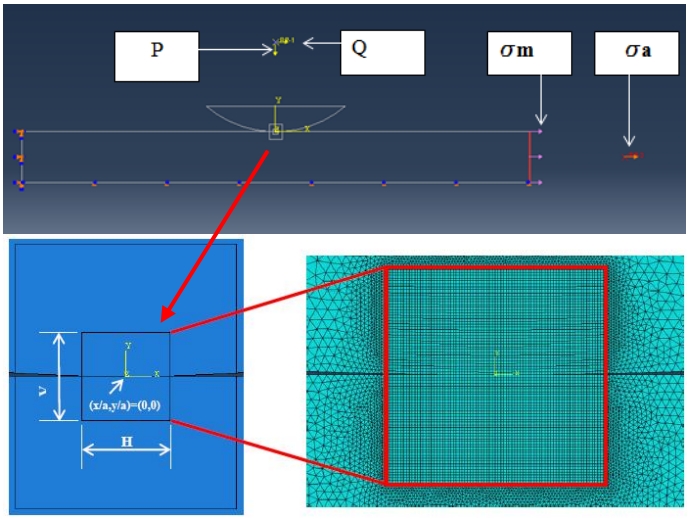

Figure 6 – Schematic view of the 2-D model and loadings that can be applied to the model.

An interactive spreadsheet was used to calculate the damage models used in this work and to solve Basquin's equations for the life estimates.

The risk of crack nucleation was investigated following the flowchart presented in Figure 7.

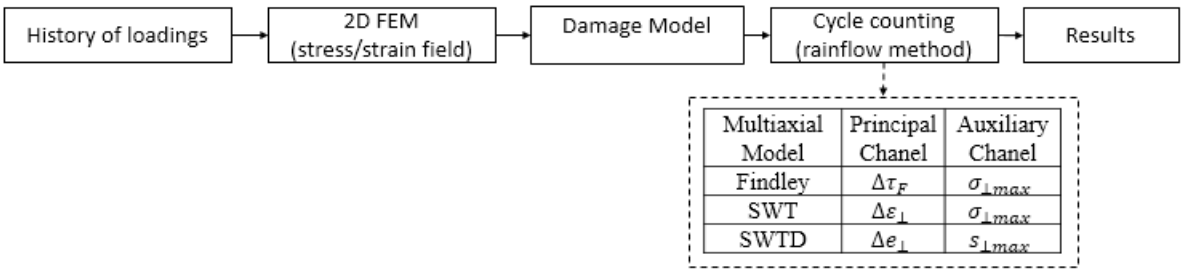

Figure 7 - Flowchart summarizing the steps used to predict the risk of crack nucleation.

5 RESULTS AND DISCUSSION

For elastic computations (LP), only one cycle sequence is requested to extract the stress loading required for the multiaxial fatigue analysis. Significant contact plastic deformation was observed for the higher pressure (HP) where $p_0/S_Y = 2.0 > 1.6$. Hence, for the elastoplastic computations, ten cycles were applied successively until reach elastic shakedown (see Figure 8) and the stabilized stress were extracted from the last cycle (10^{th} cycle).

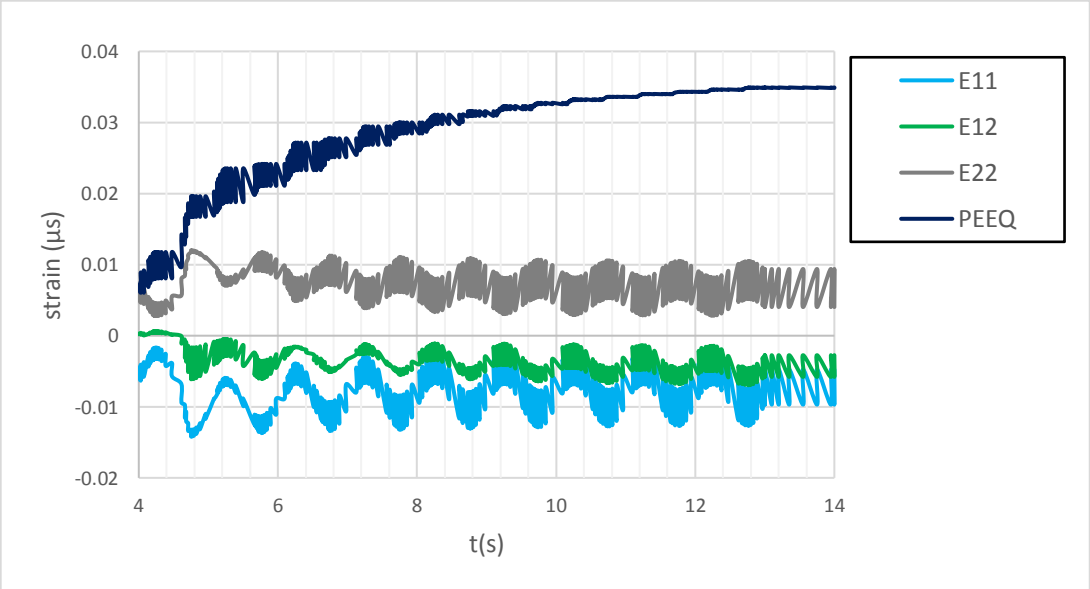

Figure 8 – Strain evolution at the hotspot with the fretting cycles (HP, R*= 40mm, P_L=540 N/mm, Q=283 N/mm).

Figure 9 shows the pressure distribution at the contact level in different steps: the pressure distribution calculated via Hertz formulation (elastic calculation), the pressure distribution at the end of normal indentation and the pressure distribution for each one of the 10 fretting cycles. Note that significant plastic accommodations were activated with the applied fretting cycles. Note the evolution of maximum contact pressure p_{max} and the contact width (2a) until reach elastic shakedown for the higher pressure (p_0 = 700 MPa). After reaching elastic shakedown, p_{max} is lower than the value calculated via Hertz model. The numerical contact width $2a_{num}$ = 1.33 is greater than a_H = 1.00 mm due to the plastic accommodation. Nevertheless, $2a_{num}$ is similar to the $2a_{exp}$= 1.45 mm reported by Fouvry at al [8] with an error smaller than 10%.

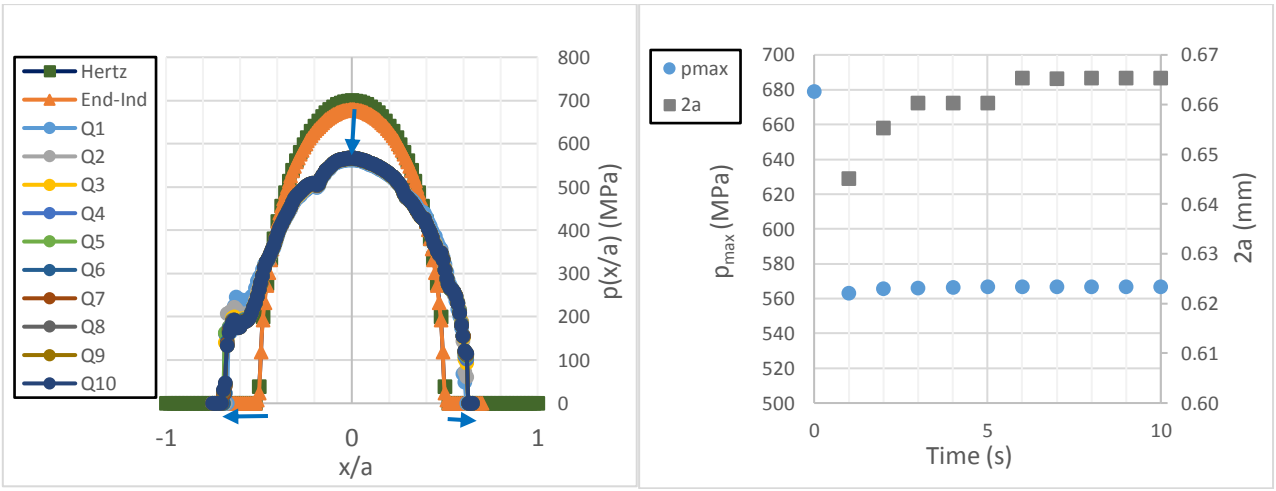

Figure 9 – Left: evolution of pressure distribution at the contact level until reach elastic. Shakedown. Right: maximum contact pressure (p_{max}) and contact width (2a) with the applied fretting cycles. (HP, R*= 40mm, P_L=540 N/mm, Q=283 N/mm).

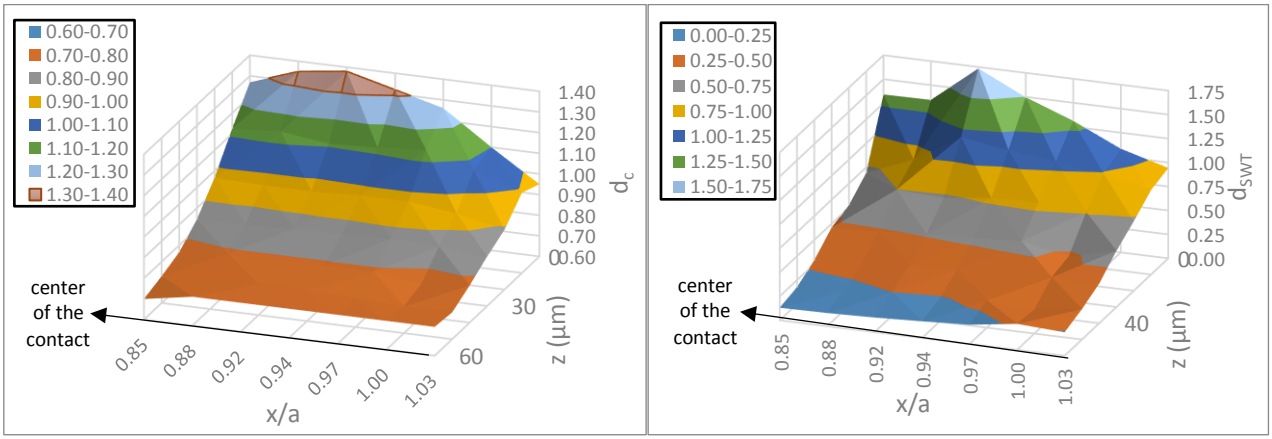

Figure 10 – Left: Crossland damage parameter. Right: SWT damage parameter at the vicinity of the contact bord (LP, R*=40 mm P=227 N/mm, Q=90N/mm).

As well known in the literature, the multiaxial damage model addressed in this paper (d_C and d_{SWT}) are maximized at the vicinity of the contact bord. Figure 10 shows both damage parameters at the vicinity of the contact for LP conditions. Note that both parameters are maximized at the point (x=-0.92a, z=0).

For HP conditions, the critical point at the surface that maximizes both damage parameters SWT and Crossland is (x=- 0.95a, z=0).

To account for the stress gradient at the contact, a non-local approach was used based on the idea of the critical distance defined in terms of the point method (L_{PM}). The critical distance was calibrated based on the experimental results presented in Table 3. A reverse analysis on the crack nucleation risk was performed considering Crossland's damage model calculated in different points beneath the critical point determined previously for LP and HP conditions.

Figure 11 presents the results for Crossland damage parameter (d_C). As described in section 2.5.1, if $d_C \geq 1$ there is a risk of crack nucleation.

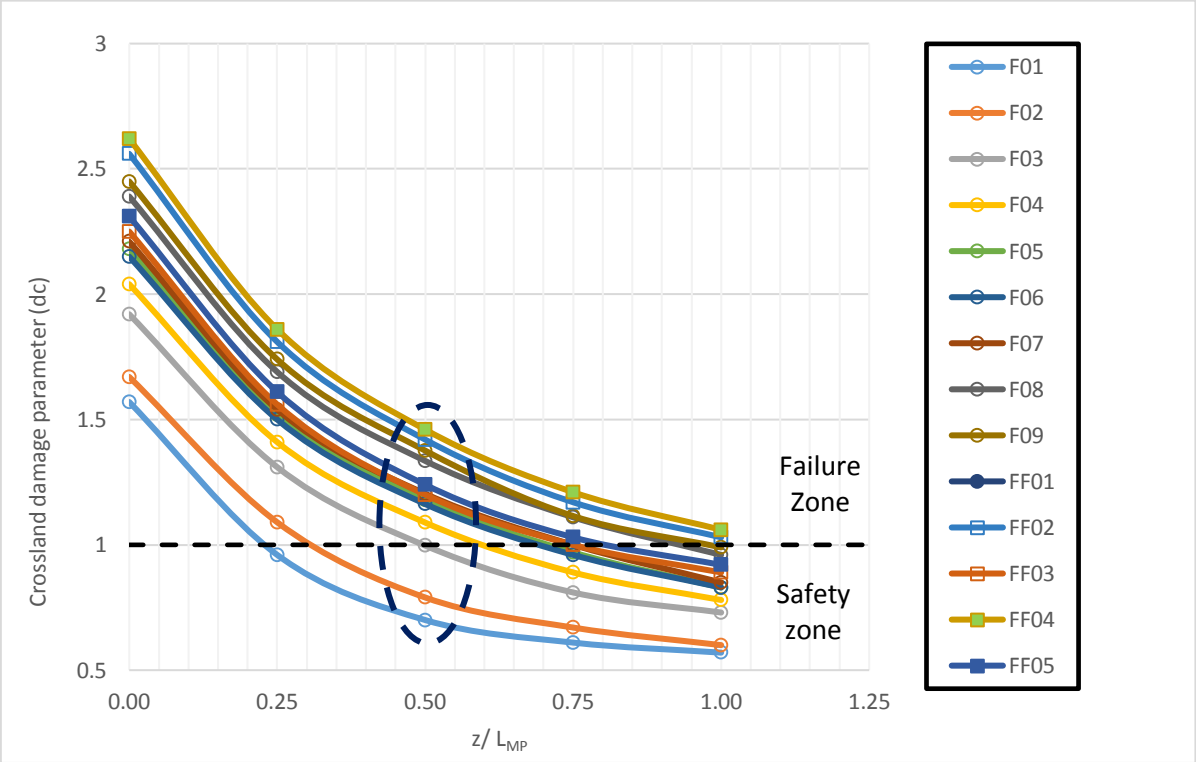

Figure 11 – Crossland damage parameter used to calibrate the Crossland critical distance L_C.

In this work, the risk of crack is presented in binary form being the number 1 used to indicate the risk of crack nucleation and 0 indicates no risk of crack. The distance that had better adjust the experimental results is $L_C = L_{PM}/2$.

It is noteworthy to point out that the use of the point method (L_{PM}) approach without being calibrated on experimental results can give non-conservative predictions on the crack nucleation risk for the studied material. Even for the test where the sample is broken (FF05), L_{PM} strategy indicates that there is no risk of crack nucleation (see Figure 11). For engineering purposes where a simple and

reliable assessment is required, determining the critical length on experimental results can be prohibitive and the point method approach must be used cautiously.

The Crossland` distance ($L_C = L_{PM}/2$) has been used by many researchers to predict fretting fatigue crack nucleation [8-10]. Crossland's model as an invariant-based model is more straightforward to be calculate because it does not require the exhaustive search for candidate planes. Nevertheless, the task of identifying the Crossland`s critical distance (L_C) can be a problem in case of lack of experimental results.

As the critical point at the surface is the same for Crossland and SWT models (see Figure 10), the critical length calibrated via Crossland model (L_C) was used combined with the critical-plane based models to predict the risk of fretting crack nucleation.

The critical-plane damage models addressed in this work were computed for two set of experimental data one for the elastic contact (lower pressure - LP) and one for elastoplastic contact (higher pressure - HP). For each set of experimental data, the risk of crack nucleation was evaluated at two different points: (i) at the critical point determined via Crossland's model and (ii) at the trailing contact bord the contact (x=- a, z=0).

5.1 Comparison with experimental data

The result of each damage model was compared with the experimental results shown previously based on the tables presented in the next sections, which includes the binary representation of crack nucleation condition (1 – risk of crack, 0 – no risk of crack), the critical plane (θ, ϕ) orientation and the number cycles to nucleate the crack.

5.1.1 Lower pressure (elastic contact)

Table 4 presents the results for the LP condition being the damage parameters calculated at the trailing contact bord (x=-a, z=0). Note that SWT damager parameter was maximized. Hence, this model should determine the critical plane orientation and the life required to the crack initiation. Nevertheless, the predictions given by SWT_D`s model and Findley`s model are the ones that better correlate the experimental results. This shows that good predictions on the crack nucleation can be obtained throughout critical-plane based models without the use of the critical length strategy. Crossland models does not require the extensively search among all candidate planes and its calculation demands lower computational cost, but the task of identifying the critical length can be prohibitive from an engineering standpoint in case of lack of experimental data.

Another point addressed is the critical plane orientation. The critical plane orientation given by SWT and SWT_D models does not reproduce the physics process of fretting crack nucleation, which was better achieved by Findley's model. As mentioned in section 3, experimental cracks are orientated toward the inner part of the contact with an angle of about 30° ± 3 to the normal to the surface. The critical-plane estimated by Findley's model was orientated with an angle about 50-60° to the normal to the contact surface (40-30° with the normal surface).

Table 4 – LP (p_0 = 450 MPa) - damage models calculated at (x=-a, z=0).

Experimental			Findley				SWT				SWT_D			
ID	Lp [μm]	*Crack risk	*Crack risk	θ (°)	ϕ (°)	N_F	*Crack risk	θ (°)	ϕ (°)	N_{SWT}	*Crack risk	θ (°)	ϕ (°)	N_{SWTD}
F01	0	0	0	0	50	1.5E+08	0	0	90	1.7E+06	0	0	90	8.3E+06
F02	0	0	0	0	50	5.0E+07	1	0	70	8.6E+05	0	0	90	3.9E+06
F03	24	1	1	170	60	9.5E+05	1	0	80	1.7E+04	1	0	80	2.9E+04
F04	29	1	1	170	60	1.3E+05	1	0	70	6.0E+03	1	0	90	6.9E+03

*1 – Risk of crack, 0 – no risk of crack.

The predictions for LP being the damage models calculated at the critical point (x=- 0.92a, z=L_{PM}/2) defined through Crossland's model are shown in Table 5. It is important to note that the predictions were non-conservative for the tests F03 and FO4 for every damage model. This suggests that the critical length defined through Crossland's model shall not be generalized (i.e., seen as a material property) and used combined with other models under elastic contact. It must be estimated for each model separately.

Table 5 – LP (p_0 = 450 MPa) - damage models calculated at (x=-0.92a, z=LC).

Experimental			Findley				SWT				SWT_D			
ID	lp [μm]	*Crack risk	*Crack risk	θ (°)	ϕ (°)	N_F	*Crack risk	θ (°)	ϕ (°)	N_{SWT}	*Crack risk	θ (°)	ϕ (°)	N_{SWTD}
F01	0	0	0	170	70	2.5E+10	0	0	80	2.1E+10	0	0	80	3.6E+09
F02	0	0	0	170	60	3.7E+08	0	170	40	1.3E+09	0	170	30	4.8E+06
F03	24	1	0	170	70	3.2E+08	0	0	70	1.0E+07	0	170	30	3.5E+07
F04	29	1	0	170	70	9.2E+07	0	0	70	1.9E+06	0	0	70	1.6E+06

*1 – Risk of crack, 0 – no risk of crack.

5.1.2 Higher pressure (elastoplastic contact)

Table 6 presents the results for HP being the damage models calculated at the trailing contact bord (x=-a, z=0). The SWT_D parameter was maximized and should define the critical-plane orientation and the estimated life for each test verified. Note that the predictions correlated well the experimental results. In the case F10, both SWT and SWT_D predictions were conservative. As verified for the elastic case, this model does not reproduce the physics of fretting crack initiation process. The predicted critical plane orientation is again normal to the surface of the contact. Once, Findley's model predictions correlated well the experimental results.

Table 6 – HP (p_0 = 700 MPa) - damage models calculated at (x=-a, z=0).

Experimental			Findley				SWT				SWT_D			
ID	Lp [μm]	*Crack risk	*Crack risk	θ (°)	ϕ (°)	N_F	*Crack risk	θ (°)	ϕ (°)	N_{SWT}	*Crack risk	θ (°)	ϕ (°)	N_{SWTD}
F10	0	0	0	0	50	8.0E+06	1	0	90	7.8E+04	1	0	90	1.0E+04
F11	14	1	1	0	50	9.9E+04	1	0	90	3.2E+03	1	0	90	3.0E+03
F12	77	1	1	0	50	1.6E+04	1	0	90	5.2E+03	1	0	90	5.0E+03
F13	61	1	1	0	50	5.0E+04	1	0	90	2.6E+03	1	0	90	3.3E+03
F14	75	1	1	0	50	1.2E+05	1	0	90	3.2E+03	1	0	90	3.0E+03

*1 – Risk of crack, 0 – no risk of crack.

Table 7 shows the results for HP being the damage models calculated at the critical point (x=- 0.95a, z=0). The SWT_D damage parameter is maximized and the predictions given by this model shows good agreement with the experimental results. It is important to note that SWT and SWT_D models yield similar results. This can be explained by the fact that locally the history of loads has moderately negative mean stresses.

In this case, it is important to note that Findley's damage parameter yields non-conservative predictions. For tensile-sensitive materials and elastoplastic contact, it would be more appropriate to choose a tensile-based model that explicitly includes $\Delta\sigma_{\perp}$.

Table 7 – HP (p_0 = 700 MPa) - damage model calculated at (x=-0.95a, z=L_C).

Experimental			Findley				SWT				SWT_D			
ID	Lp [μm]	*Crack risk	*Crack risk	θ (°)	ϕ (°)	N_F	*Crack risk	θ (°)	ϕ (°)	N_{SWT}	*Crack risk	θ (°)	ϕ (°)	N_{SWTD}
F10	0	0	0	0	40	1.3E+08	1	0	70	5.5E+05	0	0	70	3.6E+06
F11	14	1	0	0	40	3.1E+07	1	0	70	1.2E+04	1	0	70	8.0E+03
F12	77	1	0	170	70	3.4E+08	1	0	70	3.4E+03	1	0	70	2.7E+04
F13	61	1	0	170	60	3.4E+06	1	0	70	3.0E+03	1	0	70	2.3E+04
F14	75	1	0	170	70	2.9E+06	1	0	70	2.9E+03	1	0	70	2.3E+04

*1 – Risk of crack, 0 – no risk of crack.

6 CONCLUSION

A numerical study on the prediction of fretting fatigue crack nucleation was addressed in this work. Due to the properties of the materials investigated, critical-plane based damage models that accounts explicitly for the normal stresses acting on the critical plane were studied (SWT, SWT_D). In order to be coherent with the physics of fretting fatigue crack nucleation process, Findley`s model which is shear-based was also considered.

It was verified that the use of the critical distance strategy (point method) combined with Crossland's model gives good predictions on the crack nucleation when the critical distance is calibrated based on experimental results being $L_C = L_{PM}/2$. Otherwise, the predictions can be extremely non-conservative if the critical distance is defined based only on the materials properties (L_{PM}). Even for a broken specimen, the critical distance L_{PM} does not indicate risk of crack nucleation.

It was observed that the critical length should be calibrate specifically for each damage model to avoid getting non-conservative predictions. When calculated at L_C, the predictions of critical-plane based models does not give necessarily good predictions.

For the elastic contact (lower contact pressure), it was demonstrated that both Findley and SWT_D models correlated well the experimental results being these models calculated at the contact bord. This result is relevant because it avoids the use of a non-local approach such as the critical distance that needs to be calibrated based on experimental results. Furthermore, Findley`s model reproduce quite well the physics of the fretting fatigue crack process being the critical plane orientation closest to the experimental observation.

For the experimental data set with the higher contact pressure, where plastic strain dominates (LCF), SWT_D parameter shows good agreement with the experimental results when calculated at the contact bord. Furthermore, SWT_D and SWT model in this case yields similar results because locally the history of mean stresses is moderately negative. At the L_C, Findley`s model gives non-conservative predictions.

Further assessment considering different contact radius (R*) and different materials shall be investigated to corroborate the conclusions of this paper.

7 ACKNOWLEDGEMENTS

The supports provided by Capes and PUC-Rio are gratefully acknowledged.

REFERENCES

[1] R. B. Waterhouse, (1991), "Fretting Fatigue," Institute of Materials and ASM International.

[2] Suresh, S., (1998), Fatigue of materials, Cambridge University Press, 2nd edition, pp. 435-481.

[3] O'Halloran, S., Harte, A., Connaire, A., Leen, S., (2016), "The prediction of fretting fatigue in the pressure armour of dynamic flexible pipes, Offshore Technology Conference, Houston-Texas.

[4] Nowell, D., Dini, D., (2003), "Stress gradient effect in fretting fatigue", Tribology International, Vol. 36, pp. 71-78.

[5] Farris, T.N, Szolwinski, M.P, (1996), "Mechanics of fretting fatigue crack nucleation", Vol.198, pp.93-107.

[6] Taylor, D., (1999), "Geometrical effects in fatigue: a unifying theoretical model", International Journal of Fatigue, Vol. 21, pp. 413-420.

[7] Araújo, J.A., Susmel, L., Taylor, D., Ferro, J.C.T, Mamiya, E.N., (2012), "On the use of the theory of the critical distances and the modified Wöhler curve method to estimate fretting fatigue strength of cylindrical contacts", International Journal of Fatigue, Vol. 29, pp. 95-107.

[8] Fouvry, S., Nowell, D., Kubiak, K., Hills, D.A., (2008), "Prediction of fretting crack propagation based on a short crack methodology", Engineering Fracture Mechanics, Vol. 75, pp. 1605-1622.

[9] Ferré, R., Fouvry, S., Berthel, B., Amagier, A., Ruiz-Sabariego, J.A., (2013), "Prediction of fretting fatigue crack nucleation of Ti-6V-4AL/ Ti-6V-4AL interface: influence of plasticity and tensile shear fatigue properties, Procedia Engineering, Vol. 66, pp. 803-812.

[10] De Pannemaecker, A., Fouvry, S., Buffière, J.B., (2015), "Reverse identification of short-long crack threshold fatigue stress intensity factors for plain fretting crack arrest analysis", Engineering Fracture Mechanics, Vol. 134, pp 265-285.

[11] Johnson, K., (1985), Contact Mechanics, Cambridge University Press.

[12] Hills, D.A., Nowell, D., (1994), "Mechanics of fretting fatigue", Kluwer Academic Publishers.

[13] Castro, J.T.P., Meggiolaro, M.A., (2016), Fatigue design techniques: low cycle and multiaxial fatigue, Vol 2.

[14] Bannantine, J.A., Socie, D.F., (1991), "A variable amplitude multiaxial fatigue life prediction method: Fatigue under biaxial and multiaxial loading", ESIS, Vol 10, pp. 35-51.

[15] Findley, W. N., (1959)," A theory for the effect on mean stress on fatigue under combined torsion and axial load or bending", ASME, Vol 81, pp. 301-306.

[16] Smith, K. N., Watson, P., Topper, T.H., (1970), "A stress-strain function for the Fatigue of Metals", Journal Mater, Vol. 5(4), pp.767-778.

[17] Kujaswki, D. A, (2014), "A Deviatoric version of SWT parameter, International Journal of Fatigue" of SWT parameter, Vol. 67, pp.95-102.

[18] Crossland, B., (1956), "Effect of large hydrostatique pressure on the torsional fatigue strength of alloy steel", International Conference on Fatigue Metals, pp. 138-149.

[19] Castro, J.T.P., Meggiolaro, M.A., (2016), Fatigue design techniques: low cycle and multiaxial fatigue, Vol 1.

[20] Yameogo, A. (2004), Etude expérimentale et numérique de l'amorçage et de la propagation de fissures de fretting dans un assemblage roue/essieu ferroviaire. PhD thesis, Ecole Centrale de Paris.

RESPONSIBILITY NOTICE

The authors are the only responsible for the printed material included in this paper.